Proceedings of the International Gas Turbine Congress 2003 Tokyo
November 2-7, 2003

IGTC2003Tokyo TS-043

CFD Design of a 8:1 Pressure Ratio Centrifugal Compressor

Victor I. MILESHIN, Andrew N. STARTSEV and Igor K. OREKHOV

Central Institute of Aviation Motors
2, Aviamotornaya St., 111116, Moscow, RUSSIA
Phone: +7 095-362-21-94, FAX: +7 095-361-66-96, E-mail: mileshin@ciam.ru

ABSTRACT

The problem of this paper is aerodynamic design of 8:1 pressure ratio centrifugal compressor possessing high performance. Design target is to achieve 81 – 82% adiabatic efficiency for 1.5 – 2.8 kg/s corrected mass flow-rate.

This investigation is a part of research program started in 1997 consisting in N-S design and numerical evaluation with subsequent tests of centrifugal compressors of successively increasing total pressure ratio. Perfection of numerical quasi-3D design tool accompanied extensive numerical study of 3D viscous flow peculiarities. Obtained understanding generated design ideas embodied in hardware and checked experimentally.

First, this paper outlines 3D Navier-Stokes solver validation by the example of 6.5:1 total pressure ratio compressor. Then it describes impeller design procedure using quasi-3D inverse code, vaneless diffuser design based on shroud reverse flow's control and numerically obtained performances of designed 8:1 total pressure ratio compressor now put into manufacturing.

NOMENCLATURE

π^*_c	total pressure ratio of compressor
η_{ad} , ETAad	adiabatic efficiency of compressor
Q	corrected mass flow rate
Qref	reference mass flow rate (near 2 kg/s)
α,β_{blade}	blade angle, measured relative to cascade front
D	diameter
F	cross-section area
r	radius
P	static pressure
ρ	density
Ω	rotational speed of impeller
P_0	total pressure at the inlet of compressor
T_0	total temperature at the inlet of compressor
R	gas constant
k	specific heat ratio
ρ^*	critical density $=P_0/(RT_0)(2/(k+1))^{1/(k-1)}$
$(a^*)^2$	square of critical speed $=RT_0(2k/(k+1))$

Subscript

1	impeller inlet
2	impeller exit
3	vaned diffuser inlet
4	vaned diffuser outlet

INTRODUCTION

At the present time there is a strong tendency toward detailed experimental measurements and numerical analysis of 3D viscous flow field within high-pressure centrifugal compressors. This causes to anticipate that in the near future centrifugal compressor performances will be raised due to understanding of viscous flow peculiarities.

Extensive numerical practice strengthened by investigations of other authors suggests us how to control some observed viscous flow phenomena. Particular emphasis has been placed on the mouth and throat of inducer (shock pattern, control of tip leakage), on the exit of impeller (reverse flow within tip clearance), on shroud of vaneless diffuser (reverse flow) and on the semi-vaneless space of vane diffuser (inlet Mach number and flow angle spanwise distributions).

Idea applied to design the impeller tip section was to minimize passage shock intensity. It has been accomplished using concept of "supersonic diffuser with long throat" proposed by Kantrowitz (1947) which relates minimum intensity of shock wave to the length of channel ensuring shock stability to compression pulses. Considering impeller as a rotating diffuser with a long blade-to-blade channel and implementing rational passage area variations (Wadia and Copenhaver (1996)) one can construct tip cascade with different shock patterns: one-shock with supersonic flow in the throat and double-shock with two weak shock waves - ahead of the passage and at the exit of inducer. The last shock pattern corresponds to the mentioned "long-throat" concept and minimizes shock losses.

We base impeller design procedure on careful design of cascade located at 90% of blade height. To prevent choice of passage area variation and lighten the impeller design efforts, viscous CFD inverse code is called to substitute iterative search by a clear design process. This is the way to obtain adequate blading within competitive development times. Designed impeller viscous flow was checked using 3D N-S solver. Shock pattern obtained by inverse quasi-3D solver without regard for tip leakage is double-shock. But in case of 3D viscous flow the second shock wave located at the exit of inducer decays to subsonic domain of strong diffusion. Thus the term "double-compression" is used to describe the flow pattern.

Applied design and analysis codes are the software packages developed in CIAM. Experimental centrifugal compressors of 6.5:1 and 8:1 pressure ratio (not the compressor under consideration) have been tested to validate codes.

Impeller "double-compression" structure is attractive not only due to minimum shock losses but also due to minimum pressure-driven tip leakage. Tip leakage control enhances stability range of impeller.

Vaneless diffuser and impeller exit is the second region of the compressor received the designer's attention. 3D viscous flow analysis of initial design highlighted reverse flow on shroud of vaneless diffuser. Separation bubble squeezes the

Manuscript received on July 3, 2003

vaneless diffuser channel and causes unfavourable supersonic flow at the inlet of vane diffuser.

As a rule, shroud flow separation is related to high deceleration within impeller due to large exit width of impeller (see Eisenlohr et al. (2002)). To prevent excessive flow deceleration on shroud of impeller it seems useful to reduce the height of impeller blade at the exit. But in this case vane diffuser blade height becomes also reduced. It reduces stability margin of compressor at low impeller speed.

On the contrary, it is better to raise exit height and, if needed, accompany it by reduction of exit blade angle to maintain flow diffusion. Increased exit height enables to make a conical shroud of vaneless diffuser and, in the same time, maintains vane diffuser width. Vaneless diffuser conicity and increased work input due to raised blade height at the impeller exit suppress flow separation and eliminate core flow squeezing at the inlet of vane diffuser.

Detailed description of design of the 8:1 pressure ratio centrifugal compressor is preceded by 3D N-S code validation.

3D VISCOUS FLOW SOLVER

Computations were performed using "3D-IMP-MULTI" N-S solver developed in CIAM and intended for analysis of 3D viscous flow through a multi-row compressor. Finite volume discretization applies the 3rd order spatial accurate Godunov's method based on exact resolution of a Riemann problem with implicit time-marching procedure and Total Variation Diminishing concept. To treat viscous flow, the Reynolds-averaged Navier-Stokes equations closed by algebraic Baldwin-Lomax turbulence model are implemented. Viscous flow is assumed fully turbulent. Wall shear stress is determined using "wall functions" approach by assuming that the first calculation point lies in the logarithmic region of a turbulent boundary layer.

Inlet boundary conditions are total pressure, total temperature and flow angles' radial distributions. At outlet, static pressure distribution is imposed and calculated from given static pressure on hub (named backpressure) and radial equilibrium equation. Periodic boundary condition is used at periodic boundaries. Tip clearance is treated as a periodic boundary. To set boundary conditions at the interface between bladed row's flow domains, a mixing plane approach is used.

H-type grid with 32x32 points in the pitchwise and spanwise directions is used for discretization of each blade-to-blade channel (for example, the number of channels is three in case of impeller with two splitters). 3 cells are included in the tip gap.

This 3D viscous flow solver was used to calculate both flow details and map of compressor performances up to the stability limit. As is known, using steady flow solver it is not possible to simulate unsteady phenomena close to compressor surge. However, difference between numerical and experimental stall inception can be diminished by the fine step-by-step increase of backpressure. Examples of axial and centrifugal stages' 3D viscous flow analysis compared with experimental measurements have been presented in Mileshin et al. (2001).

As applied to centrifugal compressors, experimental compressors of 6.5:1 and 8:1 pressure ratio have been tested and calculated to validate the code. One of them, 6.5:1 centrifugal compressor, demonstrated the best quantitative agreement of experimental performances with computed. Fortunately, design idea of the compressor is closely related to the 8:1 centrifugal compressor design being the subject of this paper.

6.5:1 PRESSURE RATIO COMPRESSOR

The 6.5:1 total pressure ratio centrifugal compressor is intended for APU (auxiliary power unit) and consists of an axial air intake, impeller having 30 blades (15 full blades, 15 splitter blades), tandem vane diffuser having 28 blades and 68 axial guide vanes. Design data of impeller are given in Table 1.

Fig. 1 shows computed and experimental performances of the 6.5:1 total pressure ratio centrifugal compressor demonstrating satisfactory agreement of obtained data. This agreement confirms validity of the N-S solver, although for other compressors 1% discrepancy in efficiency usually takes place.

Experimental 6.5:1 compressor demonstrates high performances. At design point $\pi^*_c = 6.48$ its adiabatic efficiency is 82%. Stability margin at design rpm is more than 12%. This compressor is a good prototype for design of centrifugal compressor with 8:1 total pressure ratio.

Excellent compressor aerodynamics provides high experimental performances. Mach level lines on tip of impeller at design rotational speed (see Fig.2) explain one of the reasons of high efficiency of this compressor - low intensity shock wave located in diverging blade-to-blade channel. Pre-shock Mach number equals to 1.2. Mach level lines' trough swept from the suction side of main blade indicates tip leakage. Other reason of high efficiency is proper design of double-row vane diffuser ensuring effective total pressure recovery.

Concerning validity of the N-S solver, computed near-stall points of characteristics clarify initiation of instability of the compressor and indicate a limitation of the N-S solver.

At intermediate rotational speed (i.e. 90%, 75% and 50% of design rpm) flow calculations visualize part-span impeller stall (see fig.3). Stall region locates near impeller leading edge on shroud and grows larger as the compressor is throttled until a much larger separation zone erupts and computation process fails.

The mild and progressive nature of the phenomena at the early stage of stall development suggests that it is an incidence-caused, with separation zone extending as the compressor is throttled (see fig.3).

During the 3D viscous flow calculations the range of flow-rate, where progressive stall can take place, becomes more and more narrow as the rpm decreases. It is due to a numerical stall described by Denton (1990). According to Denton, phenomenon of numerical stall arises during the transient part of calculation and is not genuinely exist. Comparison with experimental performances (see fig.1) at 50% of design rpm reveals numerical stall. It can be seen that computed characteristic terminates at a flow-rate that is lower than experimentally measured at stability limit. Thus numerical progressive stall at low speed of impeller is a limitation of the present N-S solver.

On fig.1 for 90%, and 75% of design rpm one can find that calculated stability margins are larger than experimental. It is not the fact. Actually the left point of each characteristic is numerically unstable.

Nevertheless, at design rotational speed (see fig.1) a predominance of numerical stability margin over experimental is true, because experimental throttling had been interrupted before surge to prevent impeller failure arising from the high unsteady blade loading caused by rapidly developing pressure disturbances. Numerical instability has been accompanied by a fall of vaneless and vane diffuser total pressure recovery, whereas impeller efficiency was on the rise. Fig.4 confirms that stall of vane diffuser propagating upstream to the vaneless diffuser is the reason of this event, usually named abrupt stall.

8:1 PRESSURE RATIO COMPRESSOR

The 8:1 total pressure ratio centrifugal compressor is intended for a turbo-shaft engine and consists of a radial air intake duct with 7 struts, impeller having 33 blades (11 full blades, 11 long splitter blades and 11 short splitter blades), vane diffuser having 17 blades and 92 axial guide vanes. N-S computation predicted at design point $\pi^*_c = 8.1$ adiabatic efficiency equal to 81%. Stability margin at design rpm is more than 23%.

Table 2 contains final design data of impeller. To shape a blade of impeller, quasi-3D viscous inverse design code was used. Tip section of blade (90% of blade height) was tailored to handle a double-shock flow pattern. Being integrated into 3D blade, tip section generates 3D viscous flow in which the second

shock wave located at the exit of inducer decays to subsonic domain of strong diffusion. As expected, this "double-compression" flow pattern enhances compressor efficiency and, what is important, diminish tip leakage over an entrance region of blade passage. Fig.5 shows two non-dimensional (denominator is $\rho^*(a^*)^2$) static pressure distributions obtained from 3D viscous flow computation: custom static pressure distribution on suction and pressure sides of airfoil (90% of blade height) and distribution obtained for impeller blade with inverse designed cascade. It can be seen that "double-compression" cascade has a domain (from 0.15 to 0.35 of blade meridional length) where static pressure difference is small. Fig.6 and 7 demonstrates corresponding Mach number level lines. Tip leakage vortex is well identified as a strip of closeness of level lines for custom cascade (see fig.6). By contrast, "double-compression" cascade Mach number level lines indicate faint tip leakage vortex resulting in enhanced operating range (see fig.7).

Vane diffuser has been designed as one-row instead of double-row diffuser usually recommended for high-pressure centrifugal compressor. Apart from the fact of stability range extension, one-row diffuser allows to diminish radial size of compressor. Table 3 presents vane diffuser design data and data outlining vaneless diffuser.

Predicted performances of designed 8:1 total pressure ratio compressor are on fig.11. View of impeller is on fig.12.

In what follow we discuss some features of impeller, vaneless and vane diffuser design and review numerically obtained 3D flow structure in impeller, vaneless diffuser and vane diffuser supplementing this insight by addition of some ideas advanced in other papers.

IMPELLER BLADE DESIGN

To begin the design process initial guess of impeller blade geometry is generated to calculate initial 3D viscous flow field and axisymmetric stream surfaces. Assuming that the flow through the cascade has axisymmetric stream surfaces and that the flow on these surfaces can be treated as two-dimensional, near-shroud cascade of impeller located at 90% of the blade height is re-designed using quasi-3D viscous inverse design code (an example of redesign using quasi-3D inviscid flow inverse design solver is in Mileshin et al. (1999), quasi-3D viscous flow inverse design method is in Mileshin et al. (2003)) through modification and application of the reduced static pressure $p_{red} = p - \rho(\Omega r)^2/2$ distribution along the near-shroud section of impeller blade. As a rule, thickness of impeller is a strength analysis output and only static pressure distribution along suction side of the blade section is modified. Thus only suction side of blade section is determined aerodynamically whereas pressure side is tailored geometrically so that famous problem of blade section closeness is eliminated.

The impeller blade is developed as a ruled surface by linear connection of near-shroud and hub section points. Hub section of the impeller blade is determined geometrically by already obtained near-shroud section through the satisfaction of strength requirements (controlling the blade deviation from radial direction in the vicinity of its leading edge and so on). In doing so, hub and near-shroud sections are stacked by rotating them in the circumferential direction to achieve given lean angle of the blade trailing edge.

3D viscous flow analysis after completion of the blade design provides a guideline for the next design attempt.

As a result, at the design point, maximum relative Mach number for tip cascade of impeller is slightly more than 1.2, so that viscous boundary layer remains attached despite adverse pressure gradient and "double-compression" is constituted by a weak shock originated at the leading edge of main blade and a zone of subsonic flow deceleration in the vicinity of splitter blade. Nevertheless, at higher rotational speed (105% rpm) throat flow is supersonic (see Fig.8). As mentioned, "double-compression" impeller requires careful design to prevent leading edge shock unstart.

IMPELLER FLOW FIELD

Kang and Hirsch (1995) presented detailed information on tip leakage flow structure. They noticed that relative motion of the shroud wall generates skewing of the inlet endwall boundary layer. As a result, leakage vortex core trajectory is swept strongly from the suction side corner toward the pressure side. Because of presence of this primary tip clearance vortex, endwall boundary layer begins to separate and form a region of opposite sined vorticity, named induced vortex by Van Zante et al. (2000). The two counter rotating vortices induce a tip leakage jet between them.

Going from the design point to the stall condition, impeller's leading edge shock wave moves upstream and the value of maximum relative Mach number that is reached on the suction side of main blade increases maximizing tip leakage flow in the vicinity of impeller blade leading edge. Trajectory of tip leakage vortex sweeps from suction side. Rotor stall occurs when the tip clearance vortex trajectory comes out from the bladed passage and locates forward of the impeller leading edge (see Van Zante et al. (2000)). Fig. 7 and 10 demonstrate variation of numerically obtained impeller tip section flow patterns depending on increasing static pressure at the outlet of compressor. It can be seen (see fig.10) that at the point of the compressor's stall impeller remains un-stalled because tip clearance vortex trajectory remains within blade-to-blade channel.

Besides the tip leakage vortex trajectory, tip leakage mass flow-rate is one-more important factor defining tip leakage flow. Kang and Hirsch (1995) separate the leakage flow as pressure-driven flow and moving-wall induced flow. As mentioned, pressure-driven leakage flow can be controlled by "double-compression" static pressure distribution applied to design of tip section of impeller blade.

VANELESS DIFFUSER REVERSE FLOW

Shroud wall boundary layer flow in vaneless diffuser is highly skewed due to impeller exit flow angle. Development of the shroud secondary flow caused by radial adverse pressure gradient leads to a reverse flow occurring even at the choke point and presenting over the whole operating range.

From common practice it follows that penetration of the shroud reverse flow into the semi-vaneless space of vane diffuser is impermissible. It is due to the fact that separation bubble squeezes the channel and causes unfavourable supersonic flow at the inlet of vane diffuser. Appropriate contraction of vaneless diffuser is useful to prevent that. Unfortunately, contraction of vaneless diffuser tightens throat of vane diffuser and thereby makes the low rpm's stability range narrower.

On the other hand, it is known (Ishida et al., 2001) that shroud reverse flow region is not an actual stall cell, but the flow instability is two-fold: it arises both as incipient inducer stall cell which grows with flow-rate degradation and as hub flow recirculation upstream of the vane diffuser cascade appearing like a separation bubble on hub of the vaneless diffuser.

Careful examination of the impeller exit viscous flow suggests that region of high loss of total pressure is formed by tip leakage flow and reverse flow from the impeller exit (Ibaraki et al., 2002). However, while total pressure loss increases, the penetration of shroud reverse flow into the tip clearance space of impeller's exit causes an additional work input (Ziegler et al., 2002). Therefore increased recirculation into the impeller may enhance tendency to quick reattachment of shroud reverse flow.

Based on this insight, the following two ideas have been used for the vaneless diffuser design. The first one was to raise impeller exit blade height thus increasing impeller work input. Besides increased impeller exit height enables to make a conical shroud of vaneless diffuser without vane diffuser throat tightening. 3D N-S calculation shows that increased impeller work input and contraction of vaneless diffuser suppress flow separation on its shroud.

The second idea was to suppress shroud reverse flow by means of developing hub reverse flow region in course of the compressor throttling. It seems to increase stall margin.

Fig.9 demonstrates comparison of numerically obtained vaneless diffuser meridional streamlines generated by initial impeller exit blade height and impeller with increased blade height at the exit. Unquestionably the shroud reverse flow reattachment takes place at smaller radius in case of increased blade height.

Fig.9 also indicates jumping of reverse flow from tip at the point of maximum efficiency to hub at the point of the compressor's stall indicating that hub reverse flow suppresses shroud reverse flow.

CONCLUSION

From N-S calculation designed 8:1 total pressure ratio centrifugal compressor provides at design point π^*_c = 8.1 adiabatic efficiency equal to 81%. Stability margin at design rpm is more than 23%.

Design has been performed making the following improvements of experimental 6.5:1 compressor used as a prototype and having adiabatic efficiency equal to 82%:

1) "double-compression" impeller design increases compressor efficiency due to reduction of both shock intensity and pressure-driven tip leakage;

2) enhanced work input by raised blade height at the exit of impeller and vaneless diffuser contraction prevent flow separation on shroud of vaneless diffuser;

3) changing double-row diffuser by subsonic one-row vane diffuser provides high total pressure recovery factor, ensures wide stability range and saves radial space;

4) during compressor instability inception at design rpm vanelless diffuser flow separation attendant on abrupt stall of vane diffuser has been transferred from shroud to hub.

REFERENCES

Denton, J.D., 1990, "The Calculation of Three Dimensional Viscous Flow Through Multistage Turbomachines", ASME Paper № 90-GT-19.

Eisenlohr, G., Krain, H., Richter, F.-A., and Tiede V., 2002, "Investigation of the Flow through a High Pressure Ratio Centrifugal Compressor", ASME Paper № GT-2002-30394.

Kantrowitz, A., 1947, "The Formation and Stability of Normal Shock Waves in Channel Flows", NACA TN 1225.

Ibaraki, S., Matsuo, T., Kuma, H., Sumida, K., and Suita, T., 2002, "Aerodynamics of a Transonic Centrifugal Compressor Impeller", ASME Paper № GT-2002-30374.

Ishida, M., Sakaguchi, D., and Ueki, H., 2001, "Suppression of Rotating Stall by Wall Roughness Control in Vaneless Diffusers of Centrifugal Blowers", *ASME Journal of Turbomachinery,* Vol. 123, pp. 64-72.

Kang, S., and Hirsch, C., 1995, "Tip Clearance Flow and Loss in Axial Compressor Cascades", *CP-571, AGARD PEP 85th Symposium on "Loss Mechanisms and Unsteady Flows in Turbomachines"*, pp.10-1÷10-15.

Mileshin, V.I, Orekhov, I.K, Pankov, S.V. and Startsev, A.N., 2001, "Computational and Experimental Investigation of High-Pressure Axial and Centrifugal Compressors with Ultra-High Rotational Speed", *XV International Symposium on Airbreathing Engines, 2001, Bangalore, India, September 2-7*, ISABE-2001-1115

Mileshin, V.I, Orekhov, I.K and Startsev, A.N., 1999, "Aerodynamic Design of Axial Compressor Blading Using Quasi-3D Inviscid Techniques Checked by 3D Navier-Stokes Solver", *Proceedings of the International Gas Turbine Congress 1999 Kobe, Japan, November 14-19, 1999*, edited by Takashi Tamaru, IGTC'99 Kobe TS-24, pp.437-444.

Mileshin, V.I, Shchipin, S.K. and Startsev, A.N., 2003, "Quasi-3D and 3D Inverse Navier-Stokes Based Method Used to Design Highly Loaded Axial and Centrifugal Compressor Stages", *IGTC 2003 Tokyo, Japan, November 2-7, 2003*, edited by T.Watanabe, IGTC2003Tokyo TS-034.

Van Zante, D.E., Strazisar, A.J., Wood, J.R., Hathaway, M.D., and Okiishi, T.H., 2000, "Recommendations for Achieving Accurate Numerical Simulation of Tip Clearance Flows in Transonic Compressor Rotors", *ASME Journal of Turbomachinery,* Vol. 122, pp. 733-742.

Wadia, A.R., and Copenhaver, W.W., 1996, "An Investigation of the Effect of Cascade Area Ratios on Transonic Compressor Performance", *ASME Journal of Turbomachinery,* Vol. 118, pp. 760-770.

Ziegler, K.U., Gallus, H.E., and Niehuis, R., 2002, "A Study on Impeller-Diffuser Interaction: Part II – Detailed Flow Analysis", ASME Paper № GT-2002-30382.

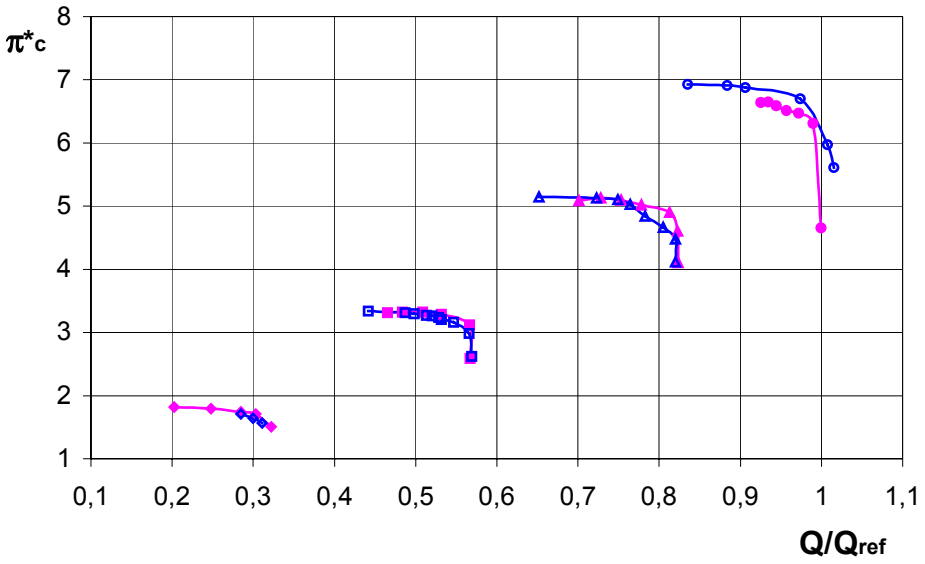

Fig. 1 Comparison of computed and experimental performances of 6.5:1 pressure ratio compressor.
Left point of each numerical characteristic is unstable. See figure continuation and legend on the next page.

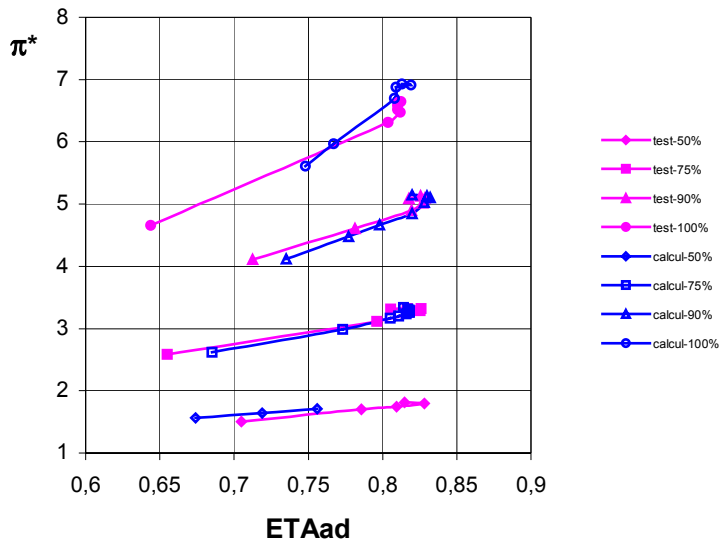

Fig. 1 Comparison of computed and experimental performances of 6.5:1 pressure ratio compressor. Continued, see previous page

Table 1. Data of impeller of 6.5:1 pressure ratio compressor

Design corrected mass flow-rate	> 2.0 kg/s
Relative hub diameter at inlet $(D_{hub}/D_{tip})_1$	0.42
Relative diameter at exit D_2/D_{tip1}	1.71
Relative axial length L_{axial}/D_{tip1}	0.513
Leading edge tip blade angle $(\beta_{blade1})_{tip}$	27°
Mean value of exit blade angle (β_{blade2})	60°
Tip speed at $\bar{n}$=1.0	570 m/s

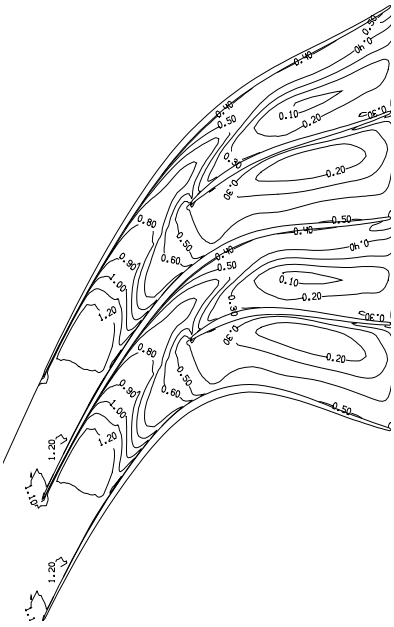

Fig.2 Mach level lines on tip. Impeller of 6.5:1 compressor. Design point, 100% rpm

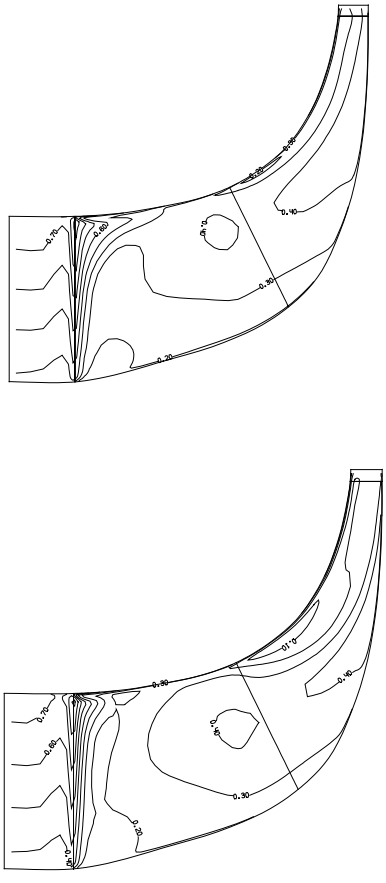

Fig.3 Mach level lines on suction surface of 6.5:1 impeller. Development of incidence-caused progressive stall at 75% rpm.
Above – maximum efficiency, below–surge.

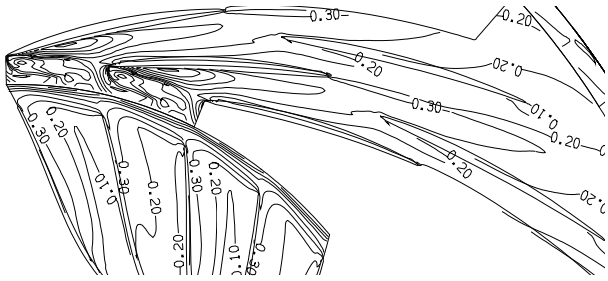

Fig.4 Mach level lines on tip. Exit of impeller and double-row vane diffuser of 6.5:1 compressor. Near-surge point, 100% rpm. Abrupt stall – stall of vane diffuser propagates upstream.

Table 2. Data of impeller of 8:1 pressure ratio compressor

Design mass flow-rate	< 2.0 kg/s
Relative hub diameter at inlet $(D_{hub}/D_{tip})_{inlet}$	0.44
Relative diameter at exit $D_2/D_{tipinlet}$	1.7
Relative axial length $L_{axial}/D_{tipinlet}$	0.427
Leading edge tip blade angle $(\beta_{1blade})_{tip}$	23°
Mean value of exit blade angle (β_{2blade})	47.8°
Tip speed at $\bar{n}$=1.0	620 m/s

Table 3. Data of vaneless & vane diffuser of 8:1 compressor

Relative length of vaneless space D_3/D_2	1.095
Angle of vaneless diffuser contraction	8°
Vane diffuser divergence F_3/F_4	2.35
Angle of equivalent diffuser (vane diffuser)	5.3°
Leading edge blade angle $(\alpha_{blade})_3$	14.8°
Exit blade angle $(\alpha_{blade})_4$	25.3°
$F_{throat\ of\ vane\ diffuser}$ / $F_{of\ flow\ at\ inlet\ of\ vane\ diffuser}$	1.055

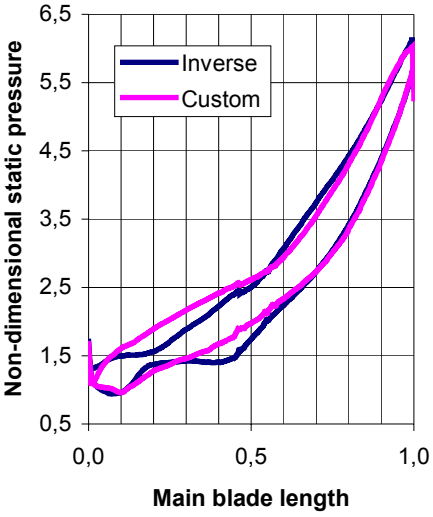

Fig.5 Comparison of non-dimensional (denominator is $\rho^*(a^*)^2$) static pressure distributions on tip of customary designed impeller and impeller designed using viscous quasi-3D inverse procedure.

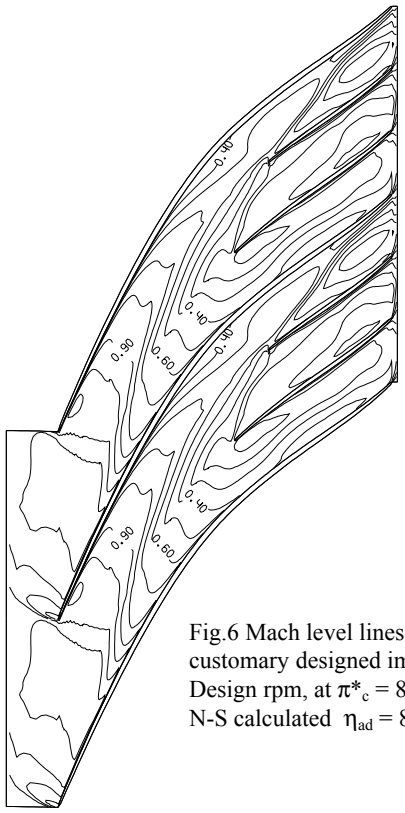

Fig.6 Mach level lines on tip of customary designed impeller.
Design rpm, at π^*_c = 8.1
N-S calculated η_{ad} = 80.4%

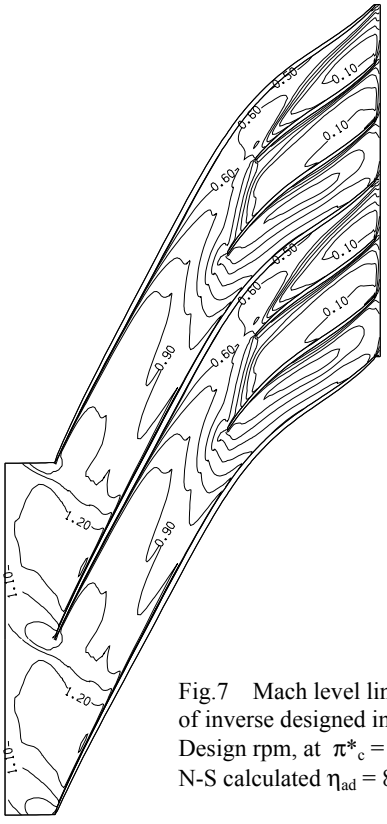

Fig.7 Mach level lines on tip of inverse designed impeller.
Design rpm, at π^*_c = 8.1,
N-S calculated η_{ad} = 81.0%

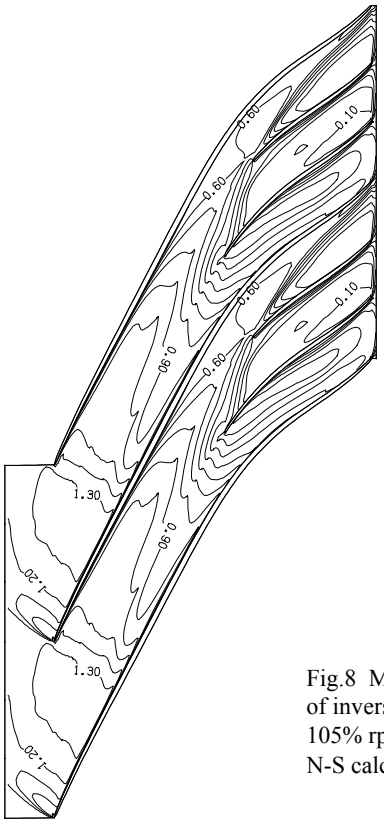

Fig.8 Mach level lines on tip of inverse designed impeller.
105% rpm, at π^*_c = 9.6
N-S calculated η_{ad} = 79.7%

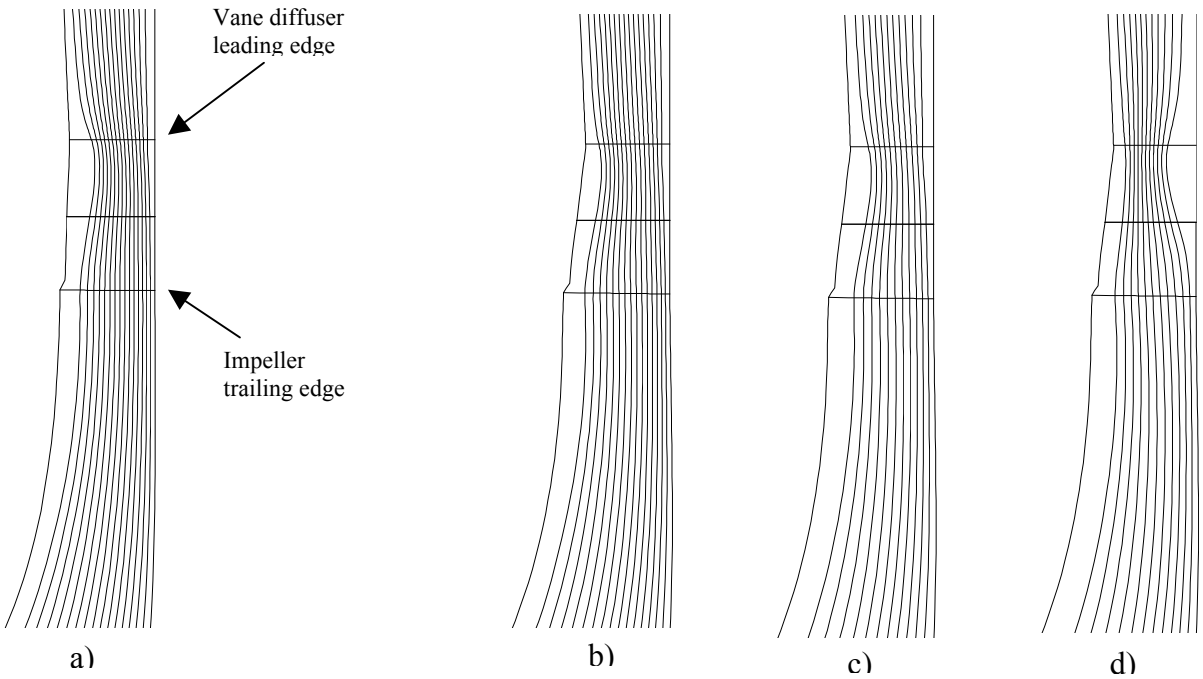

Fig.9 Meridional streamlines within vaneless diffuser of 8:1 total pressure ratio compressor at 100% rpm demonstrate effectiveness of measures to suppress vaneless diffuser reverse flow – increase of impeller exit blade height and contraction of vaneless diffuser: a) impeller with initial blade height, design point of compressor (π^*_c = 8.1, η_{ad} =81%), b) impeller with raised blade height increases work input and allows contraction of vaneless diffuser, design point of compressor (π^*_c = 8.1, η_{ad} =81%), c) raised impeller blade height, point of maximum adiabatic efficiency (π^*_c = 8.44, η_{ad} = 81.4%), d) raised impeller blade height, abrupt stall of compressor (π^*_c = 8.57, η_{ad} = 80.5%). Vane diffuser stall on hub is clearly demonstrated by streamlines departure from hub in the vicinity of vane diffuser's leading edge.

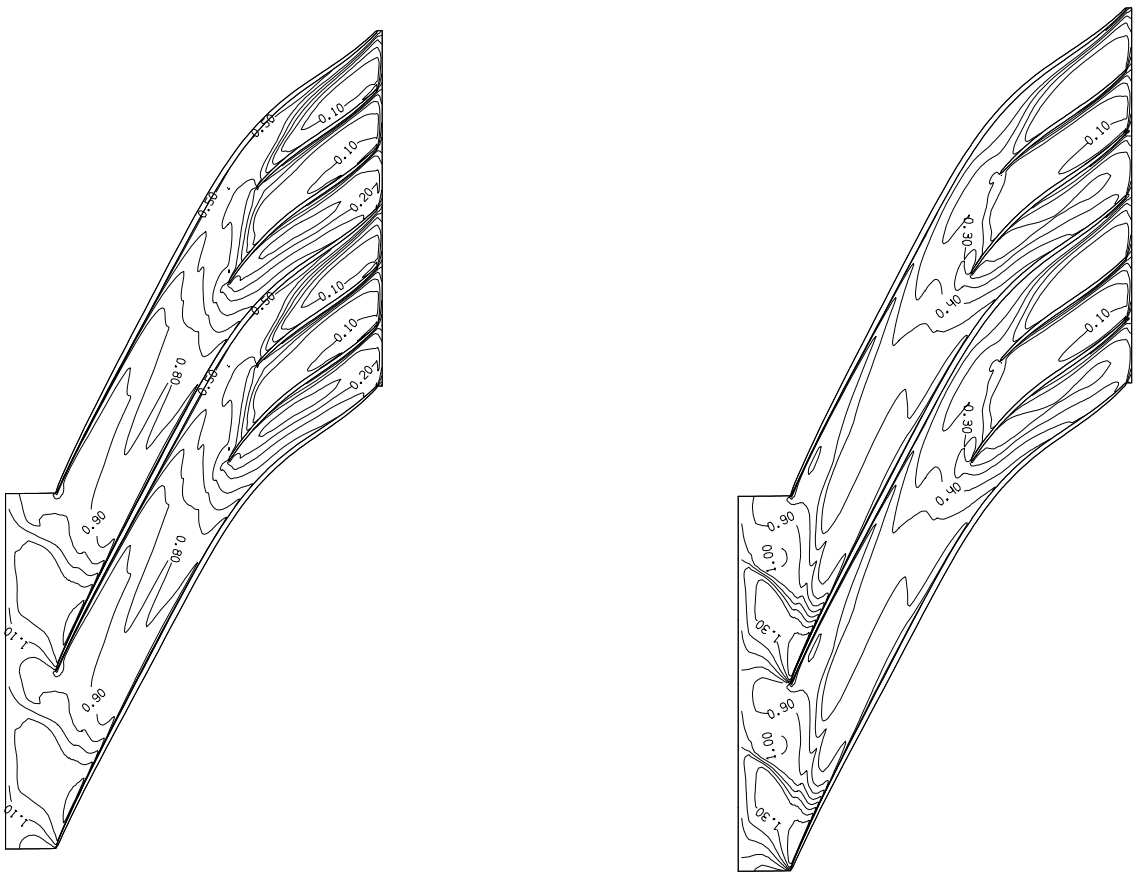

Fig.10. Mach level lines on tip of impeller of 8:1 total pressure ratio compressor. Raised impeller blade height.
Left: point of maximum adiabatic efficiency: π^*_c = 8.44, η_{ad} = 81.4%. Corresponds to Fig.9 c).
Impeller's shock wave moves upstream, but "double compression" flow pattern remains.
Right: abrupt stall of compressor: π^*_c = 8.57, η_{ad} = 80.5%. Corresponds to Fig.9 d).
Impeller's shock wave moves upstream and its intensity increases. Nevertheless, tip clearance vortex trajectory remains within impeller's bladed passage. Thus compressor surge is due to abrupt stall on hub of vane diffuser, whereas impeller is unstalled.

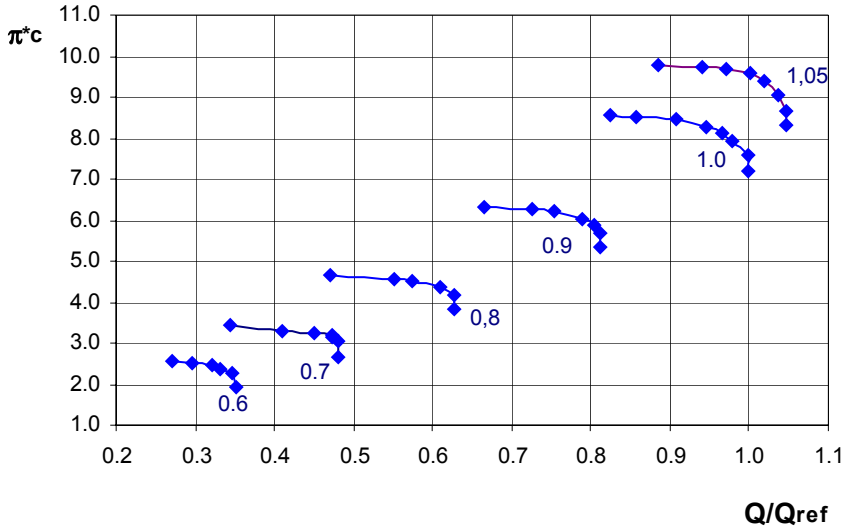

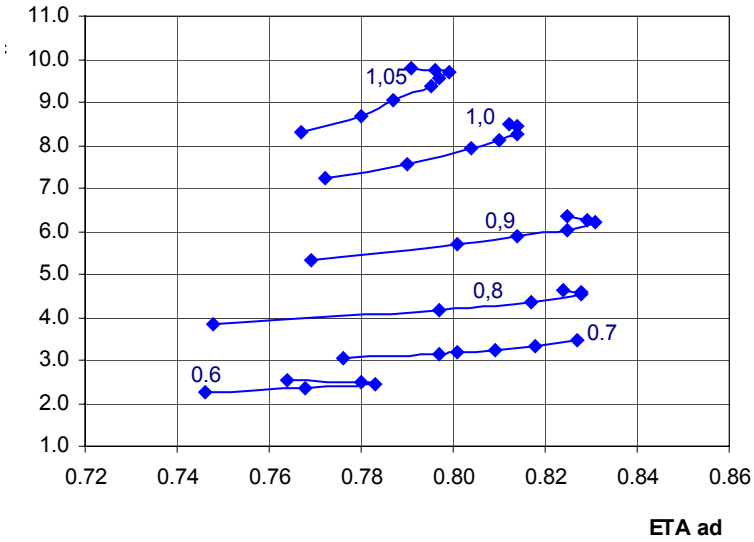

Fig.11 N-S calculated performances of designed 8:1 total pressure ratio centrifugal compressor calculated for a wide range of rotational speed of impeller n=0.6÷1.05.

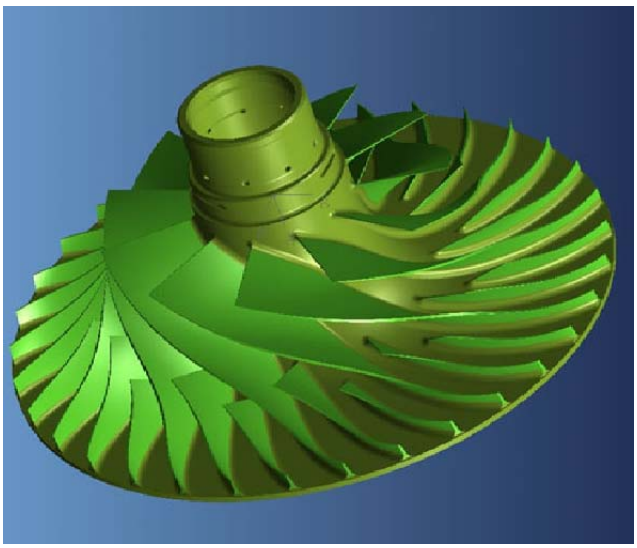

Fig.12 View of designed impeller of the 8:1 total pressure ratio centrifugal compressor